Applied Catalysis B: Environmental 125 (2012) 41–50

Contents lists available at SciVerse ScienceDirect

Applied Catalysis B: Environmental

journal homepage: www.elsevier.com/locate/apcatb

CO_2 methanation on Rh/γ-Al_2O_3 catalyst at low temperature: "*In situ*" supply of hydrogen by Ni/activated carbon catalyst

Colas Swalus[a,*], Marc Jacquemin[a], Claude Poleunis[b], Patrick Bertrand[b], Patricio Ruiz[a]

[a] *Institute of Condensed Matter and Nanosciences (IMCN), Division MOlecules, Solids and ReacTivity (MOST), Université Catholique de Louvain, Croix du Sud, 2, 1348 Louvain-la-Neuve, Belgium*

[b] *Division Bio and Soft Matter (IMCN/BSMA), Université Catholique de Louvain, Croix du Sud, 2, box L7.05.17, 1348 Louvain-la-Neuve, Belgium*

ARTICLE INFO

Article history:
Received 7 February 2012
Received in revised form 14 May 2012
Accepted 18 May 2012
Available online 27 May 2012

Keywords:
CO_2
Methanation
Rhodium
γ-Al_2O_3
Nickel
Hydrogen spill-over

ABSTRACT

Nowadays, the control of CO_2 emissions is still a challenge. A few alternatives exist but nothing concrete seems to be developed. Instead of catching and storing CO_2, one possibility would be its transformation into value added molecules as methane. Rhodium catalysts are active in CO_2 methanation reaction. But it seems that a competitive adsorption exist between the two reactants: CO_2 and hydrogen. In order to surpass this trouble and increase hydrogen adsorption, a known active catalyst in methanation (Rh/γ-Al_2O_3) was put into contact with a known active catalyst in hydrogen activation (Ni/activated carbon). Catalysts were prepared by the mechanical mixing of the latter two in different proportions. Catalysts were tested in the low temperature methanation reaction using CO_2 and H_2. Methane is produced in all cases with a 100% of selectivity. A significant synergy appears in the catalytic activity of this mixed catalyst. Production of methane in mixtures is largely higher than the theoretical predicted values considering the individual performances. Catalysts were characterized before and after reaction by ICP-AES, N_2 physisorption, XRD, CO_2 chemisorption, ToF-SIMS, XPS and TPR. The synergy is due to the increase of H_2 adsorption and promoting the carbon hydride formation. Furthermore the suggested hydrogen spill-over maintains Rh particles in a metallic state necessary for the reaction.

1. Introduction

Today, CO_2 emission is one of the major nightmares for industries and the society. A significant effort is currently done to decrease its production and release in the atmosphere. At this time, processes involving caption and underground storage of CO_2 are preferentially promoted [1]. Nevertheless, the transformation of CO_2 to high added value molecules is called to be a paramount process in the future. It opens the way to control its emissions in the atmosphere.

Nowadays, scientists are numerous to claim that the underground storage of CO_2 could be replaced, in a large part, by methanation at low temperature [2–4]. Hydrogen required for the methanation step could be obtained either from many industries which produce an excess of hydrogen or by water electrolysis. The corresponding electric energy could be furnished by means of "green" processes (solar cell panels, wind, biomass, *etc.*). In addition to converting CO_2 in a molecule of high added value, the process of transformation of CO_2 presents the advantage to convert hydrogen into a more easily exploitable source of energy, as is CH_4. Moreover the methane produced can be injected in chemical and petrochemical industries saving natural gas use. The possibility to transform H_2 and CO_2 into CH_4 becomes a real alternative in an environmental and ecological point of view.

CO_2 methanation is known for a long time and is commonly named as Sabatier reaction [1,5].

$$CO_2 + 4H_2 \leftrightarrow CH_4 + 2H_2O, \quad \Delta H^\circ = -165\ kJ\ mol^{-1}$$

The subject was recently reviewed by Wei et al. [6]. In the past, this reaction was studied by comparing CO and CO_2 methanation in high temperature conditions [7–10]. But recent results give evidences that at low temperature (<200 °C) and atmospheric pressure, the reaction takes place with very high selectivity [2,3].

Several metal catalysts have been tested in this Sabatier reaction as Rh [10–15], Ru [16,17], Ni [12,18–20] supported on different solids like Al_2O_3, SiO_2, or TiO_2. Evidences show that CO_2 adsorption and dissociation are the first steps in the mechanism of CO_2 methanation [11,17,21]. On rhodium CO_2 adsorption is largely better than the other reactant as hydrogen. Moreover, CO_2 dissociation into CO is sometimes considered as a poisoning effect on hydrogen adsorption [10,22,23]. The effect of doping supported rhodium catalysts by tungsten has been studied [14]. The increase of activity was related to the enhancement of the hydrogen adsorption capacity and by the weakening of the Rh—CO bond. Except this previous study, no attempt has tried to remediate specifically on this problem by

* Corresponding author. Tel.: +32 10473373.
E-mail address: colas.swalus@uclouvain.be (C. Swalus).

0926-3373/$ – see front matter.
http://dx.doi.org/10.1016/j.apcatb.2012.05.019

increasing the capacity of hydrogen adsorption. Nowadays, it is not stated definitively by which mechanism hydrogen reacts with dissociated species which come from CO_2. Nevertheless hydrogen is implicated in all step of CO_2 methanation mechanism. That goes to CO_2 dissociation to finally methane formation and water production [11,14]. Recent studies suggest that hydrogen could also participate to take off oxygen at the surface and to keep metal atoms in a reduced state. This reduced state is needful for CO_2 reduction [24].

In order to increase catalytic activity of the methanation, it is necessary to enhance hydrogen supply at the surface of the catalyst. It was suggested that nickel supported on activated carbon is able to stock and activate high amount of hydrogen. This hydrogen could migrate at the surface by spill-over mechanism and promoting the hydrogenation of benzene [25]. Taking advantage of nickel supported on activated carbon as a storage source of hydrogen could be useful for the reaction as the hydrogen supply is a key aspect in the activity of methanation. In fact, it could be expected that nickel supported catalysts could supply active catalysts in CO_2 methanation with activated hydrogen species to increase the reaction performances. This is the principal objective of this work. Namely, to combine a well-known catalyst in CO_2 adsorption and dissociation with a catalyst recognized in hydrogen activation. By this way, drawback in the supply of hydrogen during the methanation could be overcome.

In order to demonstrate this concept, catalysts were prepared by the mechanical mixing of the two catalysts prepared separately. The first one is nickel supported on activated carbon and the second is rhodium supported catalyst. The feasibility and the impact of an *in situ* supply of hydrogen on rhodium catalytic sites will be studied. The pure catalytic phases and the mixtures were tested in the methanation reaction using CO_2 and H_2 at low temperature. Catalysts were characterized before and after reaction by elementary analysis, N_2 physisorption, X-ray diffraction, CO_2 chemisorption, ToF-SIMS, X-ray photoelectron spectroscopy (XPS) and Temperature Programmed Reduction (TPR). In a first time, catalysts properties are studied to compare characteristics of catalysts alone and in mechanical mixtures. Next, the activity of these catalysts is highlighted in catalytic tests. Post characterisations were realized to check if some modifications occur on catalysts during the reaction. In order to complement the discussion, MoO_3 oxide and its mixture with nickel catalyst were also studied by TPR followed by XPS analyses.

2. Experimental

2.1. Catalysts preparation

2.1.1. Pure catalysts

The 1 wt.% Rh/γ-Al_2O_3 catalyst was prepared by an incipient wetness impregnation method using $RhCl_2(NH_4)_3{\cdot}H_2O$ (Acros, p.a.) as the rhodium precursor. 0.41 g of the last one were dissolved in 20 ml of distilled water at 25 °C, while 10 g of the support, γ-Al_2O_3 (Alfa Aesar, 99.97%) were added to the solution under continuous stirring at 25 °C. After agitation for 18 h at 60 °C, water was evaporated under reduced pressure in a rotavapor at 40 °C. The impregnated powder was dried in a furnace at 110 °C overnight under static air. Finally, the recovered solid was calcined at 450 °C at atmospheric pressure under static air for 2 h in a muffle furnace. Catalyst is hereafter denoted by 1 wt.% Rh/γ-Al_2O_3.

The 1% nickel supported on activated carbon catalyst was prepared by aqueous hydrazine reduction [26]. The support used was a commercial acid washed (Merck, ash content ≤ 3%) with a granulometric fraction of 40 mesh. 5 g of support were pouring in 20 ml of an aqueous solution containing 4.22 g of $Ni(CH_3COO)_2{\cdot}4H_2O$ (Aldrich, 98%). The solution was then stirred under a reflux condenser for 1 h at 80 °C. The solvent was evaporated under a reduced pressure in a rotavapor at 30 °C and dried at 80 °C in a furnace for 16 h. The reduction of the supported precursor was performed under an argon flow (Praxair, 99.2%) in a three necked reaction flask of 110 cm^3 plunged in a water bath for heating. The reaction flask was equipped with a reflux condenser and a thermocouple for temperature measurement of the reaction. A suspension of the supported nickel precursor was stirred and slowly heated to 80 °C in an excess hydrazine solution (Fluka, 24–26% in water) for 3 h at pH 10–12. After reduction the solid obtained was filtrated off, washed with distilled water and dried in air at 80 °C for 16 h. Similar procedure was followed to prepare nickel supported on activated carbon catalyst containing 0.5 wt.% and 5 wt.% of Ni. Catalysts are hereafter denoted as follows: 0.5 wt.% Ni/AC, 1 wt.% Ni/AC and 5 wt.% Ni/AC.

MoO_3 bulk catalyst was prepared by heating in air 30 g of ammonium heptamolybdate $(NH_4)_6Mo_7O_{24}{\cdot}4H_2O$ (Merck, p.a.) at 500 °C for 20 h in a muffle furnace. Catalyst is hereafter denoted by MoO_3.

2.1.2. Mechanical mixtures

Mechanical mixing between 1 wt.% Rh/γ-Al_2O_3 catalyst and nickel catalysts in different proportions were prepared. A mixture of 1 wt.% Ni/AC and MoO_3 was also prepared. The amount in weight of each solid was mixed together in about 100 ml of n-pentane (Aldrich, 99%). The mixture was stirred for 5 min and placed in an ultrasonic bath for 30 s. These operations were repeated two times. Finally, the dispersion was lightly heated to ensure evaporation of the n-pentane. Three weight ratios between 1 wt.% Rh/γ-Al_2O_3 and Ni/AC catalysts were prepared: 25:75, 50:50 and 75:25. These catalysts are denoted by (Y:Z)RhXNi where Y and Z are the fractional weight of 1 wt.% Rh/γ-Al_2O_3 catalyst and Ni/AC catalyst in the mixture respectively. X is the weight percent of Ni in Ni/AC catalysts. Only the fifty–fifty weight ratio was prepared for 1 wt.% Ni/AC with MoO_3. This sample is denoted as (50:50)Mo1Ni.

2.2. Catalytic activity measurement

2.2.1. Catalytic reactor

The reactor used consists of a fixed bed tubular flow microreactor in quartz working at 2 bar of pressure. The internal diameter of the reactor is 8 mm. The reactor was heated by a furnace controlled by a programmable temperature controller. A thermocouple placed within a quartz capillary in the middle of the catalyst bed was used to measure the temperature. The catalytic bed consisted of 0.3 g of catalyst (200–315 μm fraction) deposed on 5 mm of glass beads.

2.2.2. Pre-treatment of the catalysts and catalytic reaction

Before catalytic tests, the catalyst is first reduced *in situ* under a H_2 flow (Praxair, 99.95%) for 1 h at 350 °C. After reduction, the sample was purged in He (Praxair, 99.994%) and cooled until the reaction temperature at 125 °C. Then a pulse (volume = 1.02 cm^3) of CO_2 (Praxair, 99.998%) was introduced in the reactor using H_2 flow (Praxair, 5% in helium) as a gas carrier. Pressure was fixed to 2 bar.

2.2.3. Test in presence of helium and at high partial pressure of hydrogen

After reduction pre-treatment, a flux of helium was introduced for 30 min. Then a pulse of CO_2 was introduced using helium as gas carrier. Total pressure was 2 bar.

A test with a higher partial pressure of hydrogen was performed following similar procedure of pre-treatment but using pure hydrogen as gas carrier at atmospheric pressure.

2.2.4. Analysis of reactants and products

Input gases of 20 ml/min rates were measured by mass flow meters. Reactants and products were monitored by an online mass spectrometer equipped with a quadrupolar analyzer of Prisma type (Balzers QMS 200) at $m/z = 2$ (H_2), $m/z = 4$ (He), $m/z = 15$ (CH_4), $m/z = 18$ (H_2O), $m/z = 28$ (CO), and $m/z = 44$ (CO_2), where m/z indicates the mass to charge ratio. Data were analyzed using the Balzers Alters Quadstar 422 Measurement interface. The mass number of 15 instead of 16 was used for CH_4 to avoid interference of water and cracking of CO_2 and CO. The pressure in the chamber of analysis was 3×10^{-5} Pa. (Thermostar^{TM} PFEIFFER VACUUM). Calibration was done by injection of different known amounts of methane in the spectrometer.

2.3. Characterizations methods

2.3.1. The chemical composition of the catalyst was determined by Inductively Coupled Plasma-Atomic Emission Spectroscopy (ICP-AES) on an Iris Advantage equipment from Jarrel Ash Corporation. The samples were first brought into solution by alkali oxidative fusing $NaOH/Na_2O_2$ and subsequent dissolution with diluted HCl.

2.3.2. Textural analysis of the supports and the catalysts were carried out on a Micromeritics ASAP 2000/2010 equipment using N_2 (Praxair, 4.8) adsorption/desorption at liquid N_2 temperature, working with P/P_0 pressures in the range of 10^{-6}–1.0. Before the measurements, 150 mg of the samples were outgassed at 150 °C overnight under a 50 mTorr vacuum. BET and BJH equations were used to determine specific surface area, porous volume and pores size distribution.

2.3.3. X-ray diffraction (XRD) analyses were performed on the fresh catalyst on a Siemens D5000 diffractometer using the Kα radiation of Cu ($\lambda = 1.5418$ Å). The 2θ range was scanned between 10 and 90° by steps of $0.01° s^{-1}$. Identification of the phases was carried out using the ICDD-JCPDS database.

2.3.4. X-ray photoelectron spectroscopy (XPS) analyses were performed on an SSI X-probe (SSX-100/206) spectrometer from Surface Science Instruments. The analysis chamber was operated under ultrahigh vacuum with a pressure close to 5×10^{-9} Torr and the sample was irradiated with a monochromatic Al K_α (1486.6 eV) radiation (10 kV; 22 mA). Charge compensation was achieved by using an electron flood gun adjusted at 8 eV and placing a nickel grid 3.0 mm above the sample. Pass energy for the analyzer was 150 eV and the spot size was approximately 1.4 mm^2. For these measurements, the binding energy (BE) values were referred to the C-(C,H) contribution of the C 1s peak at 284.8 eV. The surface atomic concentrations were calculated by correcting the intensities with theoretical sensitivity factors based on Scofield cross-sections [27]. Peak decomposition was performed using curves with an 85% Gaussian type and a 15% Lorentzian type, and a Shirley non-linear sigmoid-type baseline. The following peaks were used for the quantitative analysis: C 1s, O 1s, Ni 2p, Al 2p, Rh 3d, Cl 2p and C 1s again the stability of the charge compensation. Based on the XPS analysis, the XPS surface ratio of a given element is defined as the atomic concentration of the element (%) divided by the atomic concentration of Al (%) or C (%) for rhodium and nickel catalysts, respectively. Rhodium was analyzed on $3d_{5/2}$ and $3d_{3/2}$ doublet separated from 4.74 eV. Binding energy of metallic rhodium Rh° $3d_{5/2}$ is around 307.5 eV. The fraction of rhodium in a metallic state was evaluated as the ratio between atomic surface concentration of Rh° and the total Rh concentration ($Rh°/Rh_{tot}$). XPS analysis of nickel catalysts were based on $2p_{3/2}$ and $2p_{1/2}$ doublet separated from 17.49 eV. Metallic state of nickel Ni°, NiO and Ni_2O_3 have a binding energy of 852.3 eV, 854.5 eV and 856.8 eV, respectively [28].

2.3.5. Static positive and negative ToF-SIMS measurements were performed with a ToF-SIMS spectrometer from Charles Evans and Associates [29]. The samples were bombarded with pulsed Ga^+ ions (15 keV). The secondary ions were accelerated to ±3 keV by applying a bias on the sample. The spreading of the initial energies of the secondary ions is compensated by deflection in three electrostatic analyzers. A post-acceleration of 7 keV was applied at the detector entry. The analyzed area used in this work was a square of 120 μm × 120 μm and the data acquisition time was 5 min. Charge effects were compensated by means of a pulsed electron flood gun ($E_k = 24$ eV). With these experimental settings the total ion fluence is lower than 10^{12} Ga^+ cm^{-2}, which ensures static conditions [29]. The powders were pressed on a double-face silver tape. A stainless steel grid (non-magnetic) was placed onto the sample surface in order to prevent variations of the surface potential.

2.3.6. CO_2 chemisorption measurements were performed on a Micromeritics ASAP 2010 Chemi apparatus. The U-shaped sample tube containing 0.2 g of the catalyst was first flushed under a H_2 flow at 350 °C for 1 h to reduce the catalyst. Then, the sample was flushed with a He flow at 25 °C for 2 h. Finally the sample was evacuated at 25 °C for 2 h down to a residual pressure of <5 μmHg. The first CO_2 adsorption isotherm was recorded at 125 °C. Then the sample was flushed under He at 80 °C and the second CO_2 adsorption isotherm was measured at 125 °C. The difference between the two isotherms corresponds to the amount of carbon dioxide chemisorbed on the samples at 125 °C. The results were expressed in terms of cm^3 of chemisorbed CO_2 per gram of catalyst.

2.3.7. Temperature programmed reduction (TPR) was performed in a fixed bed quartz tube. The catalytic bed consisted of 0.1 g of catalyst deposed on 5 mm of glass beads and surmounted by a layer of approximately 3 mm of glass beads. Outlet gases were analyzed by an online mass spectrometer (Balzers QMS 200) equipped with a quadrupolar analyzer of Prisma type. The pressure in the chamber of analysis was 3×10^{-5} Pa. The catalyst was initially purged with helium (Praxair, 99,999%) at a flow rate of 60 ml min^{-1} and heated up to 300 °C at a ramping rate of 7.5 °C min^{-1}. After cooling down to ambient temperature, the catalyst was placed into a hydrogen flow (Praxair, 5% in helium) with a rate of 10 ml min^{-1}. Then, temperature was increased to 150 °C by a slope of 7.5 °C min^{-1}. Reduction of the catalyst was detected on the spectrometer by water ions production $m/z = 18$.

3. Results

3.1. Activity measurements

3.1.1. Mixture of 1 wt.% Rh/γ-Al_2O_3 with Ni/AC catalysts

At 125 °C, the selectivity in hydrocarbon compounds is 100%. The only hydrocarbonated compound detected is methane. Water is also observed during the methanation reaction. Results are showed in Fig. 1. Methane production is expressed in μmoles of methane per gram of catalyst (μmol g^{-1}) and in μmoles of methane produced by gram of 1 wt.% Rh/γ-Al_2O_3 catalyst present in the mixture (μmol g_{Rh}^{-1}). Predicted theoretical values for methane production by catalyst alone (not in the mixture) are represented by the black line. These values were calculated admitting that the catalytic activity is proportional to the amount of catalysts contained in the mixture. 1 wt.% Ni/AC catalyst presents no catalytic activity for the reaction whereas 1 wt.% Rh/γ-Al_2O_3 catalyst and mechanically mixing catalysts are highly active. Methane production per gram of 1 wt.% Rh/γ-Al_2O_3 catalyst (μmol g^{-1}) increases with a diminution of 1 wt.% Rh/γ-Al_2O_3 in the mixing. Clearly an important synergetic effect is observed by the mixture of 1 wt.% Rh/γ-Al_2O_3 with 1 wt.% Ni/AC catalyst. Production of methane is largely higher than the calculated predicted values.

The results obtained for the three mixtures of 1 wt.% Rh/γ-Al_2O_3 with 0.5 wt.% Ni/AC, with 1 wt.% Ni/AC and with 5 wt.% Ni/AC are presented in Table 1. The better performances are observed for

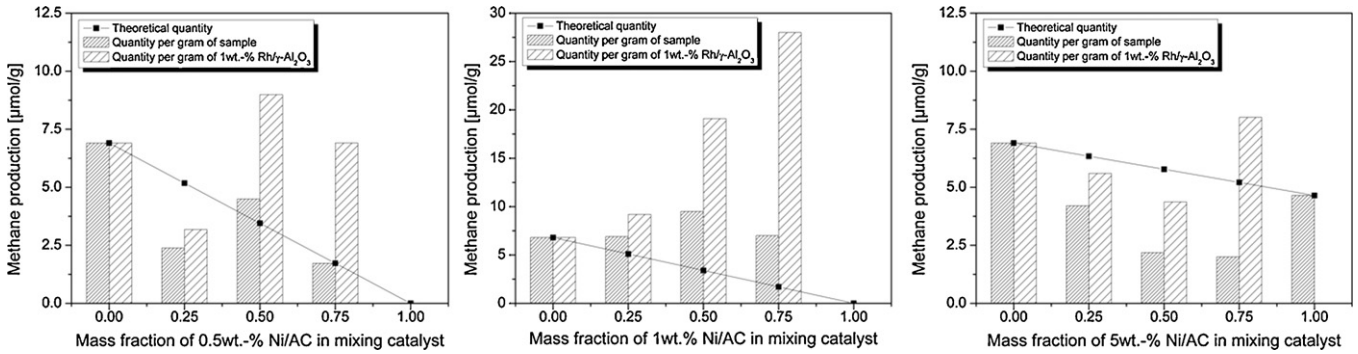

Fig. 1. The methane production is expressed in function of the mass fraction of Ni/AC in the mixtures. A synergy effect appears for the mixed catalysts. The CH_4 produced per gram of 1 wt.% Rh/γ-Al_2O_3 in mixing is higher than the calculated value for 1 wt.% Rh/γ-Al_2O_3 alone (Conditions: 125 °C, 2 bar).

Table 1
Catalytic activity in methanation reaction at 125 °C and 2 bar. Pulse of CO_2 with a carrier containing 5% of H_2 at 2 bar of pressure.

Catalyst	CH_4 produced by gram of catalyst [$\mu mol\, g^{-1}$]	CH_4 produced by gram of 1 wt.% Rh/γ-Al_2O_3 [$\mu mol\, g_{Rh}^{-1}$]	Conversion [%]
1 wt.% Rh/γ-Al_2O_3	6.8	6.8	6
(75:25)Rh0.5Ni	2.3	3.1	2
(50:50)Rh0.5Ni	4.4	8.8	4
(25:75)Rh0.5Ni	1.7	6.8	1
0.5 wt.% Ni/AC	No active	–	0
(75:25)Rh1Ni	6.9	9.2	6
(50:50)Rh1Ni	9.5	19.1	8
(25:75)Rh1Ni	7.0	28.0	6
1 wt.% Ni/AC	No active	–	0
(75:25)Rh5Ni	4.1	5.5	3
(50:50)Rh5Ni	2.1	4.3	2
(25:75)Rh5Ni	2.0	7.9	2
5 wt.% Ni/AC	4.6	–	4

the mixture 1 wt.% Rh/γ-Al_2O_3 + 1 wt.% Ni/AC. For the other mixtures the production of CH_4 by gram of catalyst ($\mu mol\, g^{-1}$) and the CH_4 produced by gram of 1 wt.% Rh/γ-Al_2O_3 ($\mu mol\, g_{Rh}^{-1}$) are lower. It is observed that a maximum of the CH_4 produced by gram of 1 wt.% Rh/γ-Al_2O_3 is observed for the mixture (50:50)Rh0.5Ni, (25:75)Rh1Ni and (25:75)Rh5Ni. Note that a small methane production is observed for 5 wt.% Ni/AC catalysts.

3.1.2. Test in presence of helium and high partial pressure of H_2

No methane is formed when helium is used as carrier of CO_2. The catalyst is completely inert. When the carrier of CO_2 is 5% H_2 diluted in helium, catalysts are active. For pure H_2, the activity is improved significantly. Clearly, the methanation reaction depends on the partial pressure of hydrogen. Results are presented in Table 2.

3.2. Catalyst characterization

3.2.1. ICP-AES analyses

For 1 wt.% Rh/γ-Al_2O_3, 0.5 wt.% Ni/AC and 1 wt.% Ni/AC, the experimental metal loadings on the supports agree well with the expected values calculated from the amount of each reactant included during the synthesis. For 5 wt.% Ni/AC the experimental metal loading was 50% lower. Filtration step after hydrazine reduction could be responsible for this loss. Results are presented in Table 3.

Table 2
Catalytic activity results of 1 wt.% Rh/γ-Al_2O_3 catalyst. Experiments performed by introducing CO_2 pulse with a carrier of 5% of H_2 in helium, and with a carrier of pure H_2. Temperature = 125 °C.

Carrier	Pressure [bar]	CH_4 produced by gram of catalyst [$\mu mol\, g^{-1}$]	Conversion of CO_2 [%]
5% H_2 in He	2	7	6
Pure H_2	1	61	50

3.2.2. N_2 physisorption

Results obtained by nitrogen physisorption are presented in Table 3 for γ-Al_2O_3, 1 wt.% Rh/γ-Al_2O_3, activated carbon (AC) and Ni/AC catalysts. First, for these samples, no significant differences are observed during the synthesis between the support and the catalyst, except for 1 wt.% Rh/γ-Al_2O_3 catalyst. In this case, the pores diameter lightly increases. Second, rhodium catalyst possess mesopores of about 27 nm with a small specific area (79 $m^2\, g^{-1}$). Conversely, Ni/AC catalysts are composed of micropores of about 2 nm with a very high specific surface area.

3.2.3. XRD

On 1 wt.% Rh/γ-Al_2O_3 the only phase observed is the γ-Al_2O_3 phase (JCPDS – nº. 47-1308). No metallic or oxide structure of rhodium is observed. XRD patterns for the catalysts with 1 wt.% Ni/AC do not show peaks which could come from metallic nickel particles.

3.2.4. X-ray photoelectron spectroscopy (XPS)

XPS analyses were done after synthesis, after hydrogen reduction and after catalytic test. Results for rhodium catalyst, nickel catalysts and the mixtures with 50% in weight of each catalyst are presented in Tables 4–6 respectively.

From Table 4 it is observed that C/Al and O/Al remain constant after reduction and after test. The fraction of rhodium in a metallic state is determined as the ratio between atomic surface concentration of Rh° and the total Rh concentration. The XPS spectrum of the 1 wt.% Rh/γ-Al_2O_3 is presented in Fig. 2. Rh° is attributed to a component of Rh $3d_{5/2}$ with a binding energy between 307.2 and 307.5 eV and for $Rh^{\delta+}$ a component with a binding energy of

Table 3
ICP-AES elementary analyses and nitrogen physisorption analyses of γ-Al_2O_3, 1 wt.% Rh/γ-Al_2O_3, activated carbon and nickel catalysts.

Sample	Experimental metal loading [wt.%]	Specific surface area [$m^2\ g^{-1}$]	Mesoporous volume [$cm^3\ g^{-1}$]	Microporous volume [$cm^3\ g^{-1}$]	Pores diameter [nm]
γ-Al_2O_3	–	79	0.2	0.005	13
1 wt.% Rh/γ-Al_2O_3	1.1	79	0.5	0.006	27
Activated carbon (AC)	–	1263	0.5	0.300	2
0.5 wt.% Ni/AC	0.5	1117	0.5	0.300	2
1 wt.% Ni/AC	0.9	1275	0.5	0.300	2
5 wt.% Ni/AC	2.4	1058	0.5	0.300	2

Table 4
XPS analysis of 1 wt.% Rh/γ-Al_2O_3.

Sample	Treatment	C/Al	O/Al	Rh/Al	Cl/Al	Rh°/Rh_{tot}	Rh° [eV]	$Rh^{\delta+}$ [eV]
γ-Al_2O_3	Fresh	0.23	1.60	*	*	*	*	*
1 wt.% Rh/γ-Al_2O_3	After synthesis	0.29	1.68	0.007	0.011	13%	307.2	309.4
1 wt.% Rh/γ-Al_2O_3	After reduction	0.24	1.68	0.006	0.007	82%	307.5	309.5
1 wt.% Rh/γ-Al_2O_3	After catalytic test	0.28	1.57	0.007	0.005	66%	307.5	309.4

* No peak.

Table 5
XPS analysis of 1 wt.% Ni/AC.

Sample	Treatment	O/C	N/C	Ni/C	Ni $2p_{3/2}$ [eV]	Ni $2p_{3/2}$ [eV]
Activated carbon	Fresh	0.12	0.002	*	*	*
1 wt.% Ni/AC	After synthesis	0.65	0.006	0.12	857.0	*
1 wt.% Ni/AC	After reduction	0.37	0.002	0.07	856.8	853.7
1 wt.% Ni/AC	After catalytic test	0.42	0.002	0.09	856.9	853.5

* No peak.

309.4–309.5 eV. The rhodium ratio in a metallic state increases from 13% after synthesis to 82% after a reduction by hydrogen at 350 °C in the reactor. After reaction the fraction of Rh°/Rh_{tot} decreases to 66%. Note that a small amount of chloride was observed in the sample after synthesis but drop after the reduction.

The XPS Ni/C ratio is 0.12 for the fresh catalyst (Table 5). This value decreases after the reduction and test. The O/C and N/C atomic ratio decrease also after these steps. The decomposition of nickel peaks to determine the nickel state is not obvious. Only a new small peak is observed at 853.7 eV after reduction of catalysts. This peak is attributed to a slight decrease of the oxidation state of nickel atoms. Quantification of nickel in a metallic state is thus not possible. Nevertheless the presence or the absence of this peak is an indication of some reduction of nickel atoms. Based on this hypothesis, a shouldering of the nickel peak is observed after the reduction of the catalyst before a catalytic test. This is consistent with the hydrogen treatment.

Results obtained with the mixture (50:50)Rh1Ni are presented in Table 6. By comparison with separated 1 wt.% Rh/γ-Al_2O_3 and 1 wt.% Ni/AC catalysts, the results obtained with the mechanical mixtures are quite similar. The XPS Rh/Al atomic ratio after reduction and the test remain at the same values as in 1 wt.% Rh/γ-Al_2O_3. The XPS Ni/C atomic ratio decreases to similar value after reduction and after test as in 1 wt.% Ni/AC. For the mixture, the percentage of rhodium atoms in a reduced state increases during the reduction step from 16% to 70% and decreases slightly till 65% after the test. In both cases, a part of rhodium particles is thus re-oxidized during a catalytic test. Nickel catalysts follow the same tendency. Nickel particles are re-oxidized after a catalytic test. The small peak at 853.7 eV which has been assigned to some reduced nickel particles is not observed after reaction.

For the mixtures (50:50)Rh0.5Ni and (50:50)Rh5Ni (Table 6), the XPS Rh°/Rh_{tot} atomic ratio increases respectively from 13% to 75% and from 5% to 74% after the reduction treatment. After reaction the fraction of XPS Rh°/Rh_{tot} atomic ratio decreases in a similar way in both cases (64% and 69% respectively). These values are also similar to those observed for the mixtures (50:50)Rh1Ni (65%) and pure 1 wt.% Rh/γ-Al_2O_3 (66%). Then in both three mixtures, independent of the Ni content in Ni/AC catalyst, the XPS Rh°/Rh_{tot} atomic ratio after test is about the same.

Table 6
XPS analyses of mixed catalysts.

Sample	Treatment	O/Al	O/C	Rh/Al	Ni/C	Rh°/Rh_{tot}	Ni^δ/Ni_{tot} [a]
(50:50)Rh0.5Ni	After synthesis	1.7	1.9	0.008	0.009	13%	*
(50:50)Rh0.5Ni	After reduction	1.6	2.0	0.005	0.004	75%	*
(50:50)Rh0.5Ni	After catalytic test	1.6	2.0	0.006	0.007	64%	*
(50:50)Rh1Ni	After synthesis	1.6	1.7	0.006	0.015	16%	*
(50:50)Rh1Ni	After reduction	1.6	1.5	0.007	0.009	70%	0.12
(50:50)Rh1Ni	After catalytic test	1.7	1.7	0.007	0.010	65%	*
(50:50)Rh5Ni	After synthesis	1.6	2.3	0.007	0.026	5%	*
(50:50)Rh5Ni	After reduction	1.5	2.1	0.005	0.009	74%	0.14
(50:50)Rh5Ni	After catalytic test	1.7	2.3	0.006	0.015	69%	0.04

[a] Composante of Ni^δ where $0 < \delta < 2$.
* No peak.

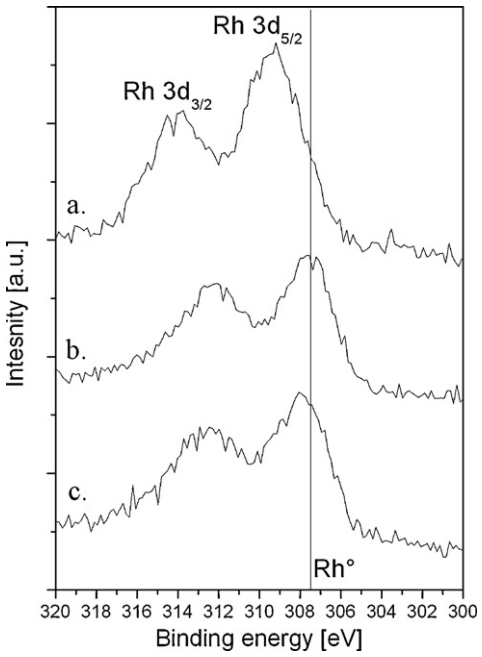

Fig. 2. Rh_{3d} XPS spectra for 1 wt.% $Rh/\gamma\text{-}Al_2O_3$ catalyst (a) after synthesis (b) after reduction and (c) after catalytic test. Reduction of rhodium particles are observed after the reduction step and slightly oxidized during catalytic test.

3.2.5. ToF-SIMS analysis

In order to investigate the probable modifications occurred at the extreme surface of the catalysts during the mechanical mixing synthesis ToF-SIMS measurements were done. Rhodium, nickel and mixed catalysts were analyzed.

Fig. 3 presents a positive ions spectrum ToF-SIMS measurement of 1 wt.% $Rh/\gamma\text{-}Al_2O_3$ after reaction. Similar spectrum was observed for the catalyst after synthesis and after reduction. Characteristics ions of metallic particles and organic compounds are detected. Rhodium catalyst shows characteristics ions of alumina and rhodium like Rh^+ ($m/z = 103$) but also some organometallic traces of $RhCH_3^+$ and $RhC_2H_3^+$ and organic compounds as $C_8H_5O^{3+}$. The negative ions spectrum shows few chloride impurities as Cl^-, $RhCl^-$, $RhClO^-$, $RhCl_2^-$ and ions as AlO^-, Al_2O^-. Several hydrocarbons as $C_2H_5^+$, $C_3H_5^+$, $C_4H_9^+$, *etc.* were also detected.

The positive ions spectrum of fresh 1 wt.% Ni/AC catalysts are presented in Fig. 3. The ions corresponding to Ni^+, Ni^{2+}, $NiOH^+$, Mg^+, Si^+, Na^+, Ca^+, Fe^+ were observed. As in the case of 1 wt.% $Rh/\gamma\text{-}Al_2O_3$, traces of organometallic compounds as $NiCH_3^+$ are detected. Measurements on the mechanical mixing catalysts do not put other ions in evidence. Similar fragments are distinguished for fresh, reduced and after test on 1 wt.% $Rh/\gamma\text{-}Al_2O_3$, 1 wt.% Ni/AC and their mechanical mixtures. No fragments composed of nickel and rhodium atoms are detected. These results suggest strongly that the catalysts are not modified by the mechanical mixture preparation, the reduction step or the catalytic test.

3.2.6. Chemisorption of CO_2

The capacity of 1 wt.% $Rh/\gamma\text{-}Al_2O_3$ catalyst to adsorb CO_2 on its surface was studied by CO_2 chemisorption analysis. This technique permits to estimate that 0.3 cm^3 of CO_2 are adsorbed per gram of catalyst at 125 °C at atmospheric pressure. That corresponds to 6.3 μmol of CO_2 per gram of catalyst. On alumina support, 0.2 cm^3 of CO_2 per gram of alumina were adsorbed. That corresponds to approximately 65% of CO_2 adsorption detected on 1 wt.% $Rh/\gamma\text{-}Al_2O_3$ catalyst. As activated carbon for hydrogen, alumina induces the adsorption of CO_2 during the reaction on its surface. Experiments done on carbon and Ni/AC catalysts indicate that no chemisorption of CO_2 occurred on these materials. CO_2 is only physisorbed on Ni/AC and a flush of helium at 80 °C desorbs easily all the CO_2. These results confirm the different and opposite affinity of the catalysts for CO_2 adsorption.

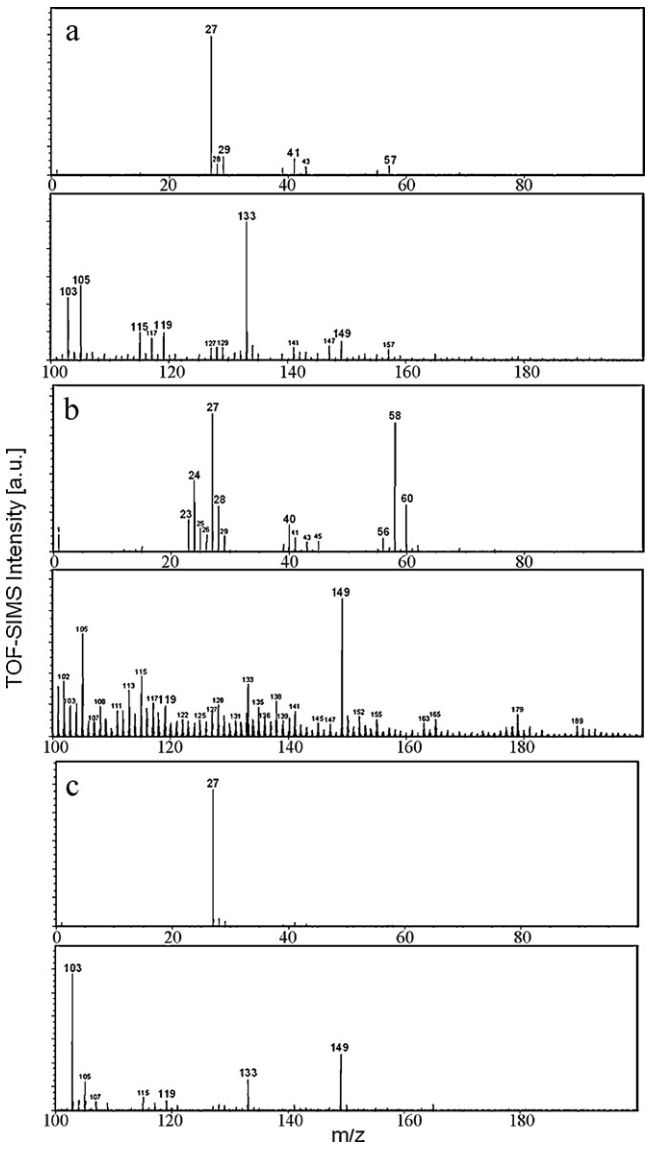

Fig. 3. Positive ions analysis by ToF-SIMS on (a) fresh 1 wt.%$Rh/\gamma\text{-}Al_2O_3$ catalyst, (b) 1 wt.% Ni/AC and (c) (50:50)Rh1Ni. No difference appears during treatments as reduction or catalytic test.

3.2.7. Temperature Programmed Reduction (TPR)

TPR was used to determine the differences in terms of H_2 activation and catalysts reduction behavior between separated and mixed catalysts. 1 wt.% $Rh/\gamma\text{-}Al_2O_3$, 1 wt.% Ni/AC and the mixture (50:50)Rh1Ni sample were analyzed. Results are show in Fig. 4. The reduction of 1 wt.% Ni/AC is very low. Inversely the formation of water is significantly higher for 1 wt.% $Rh/\gamma\text{-}Al_2O_3$. At lower temperature (<125 °C), the formation of water of 1 wt.% $Rh/\gamma\text{-}Al_2O_3$ is about the same for the mixture. At higher temperature (>125 °C), the mixing of catalysts involves an important increase in water production compared to pure catalysts. This increase of water could be relied on an increase of hydrogen adsorption and reaction in the catalytic mixture.

XPS results of the TPR samples are presented in Table 7. The reduction at 150 °C of 1 wt.% $Rh/\gamma\text{-}Al_2O_3$ sample increases the

Table 7
XPS analysis of samples before and after TPR analysis of 1 wt.% $Rh/\gamma\text{-}Al_2O_3$, 1 wt.% Ni/AC and the mixture (50:50)Rh1Ni.

Sample	Treatment	Rh/Al	Rh/C	Ni/C	Ni/Al	Rh°/Rh_{tot}
1 wt.% $Rh/\gamma\text{-}Al_2O_3$	After synthesis	0.006	*	*	*	9%
1 wt.% $Rh/\gamma\text{-}Al_2O_3$	After reduction at 150 °C	0.007	*	*	*	30%
1 wt.% Ni/AC	After synthesis	*	*	0.06	*	*
1 wt.% Ni/AC	After reduction at 150 °C	*	*	0.10	*	*
(50:50)Rh1Ni	After synthesis	0.007	0.03	0.04	0.015	11%
(50:50)Rh1Ni	After reduction at 150 °C	0.007	0.02	0.02	0.008	31%

* No peak.

amount of metallic Rh atoms (from 9 to 30%). The 1 wt.% Ni/AC catalyst seems not reduced at all. No metallic nickel atoms is observed. For the mechanical mixtures, the XPS C/Al (0.66) and Rh/C (0.03) atomic ratios remain unchanged after reduction. The XPS Ni/Al and Ni/C atomic ratios decrease after reduction. A loss in the dispersion of Ni is observed. The XPS Rh°/Rh_{tot} atomic ratio increases after reduction. The fraction of metallic Rh, in the mixture increases after reduction from 11 to 31%. No metallic Ni is observed. It remains unchanged after the reduction alone or in mixture with 1 wt.% $Rh/\gamma\text{-}Al_2O_3$.

MoO_3 catalyst and the mixture (50:50)Mo1Ni catalysts were also studied. Results are presented in Fig. 5. Pure MoO_3 and 1 wt.% Ni/AC catalysts seems to have no significant reduction before 250 °C. Result for mechanical mixture is dramatically different. Water production is considerably higher at low temperature for the mixture. The 1 wt.% Ni/AC promotes the reduction of MoO_3.

XPS analyses were realized on MoO_3, 1 wt.% Ni/AC and mixing samples after TPR treatment (Table 8). The amount of molybdenum as Mo^{5+} increase to 31% for MoO_3 alone and of 40% for mixed catalyst respectively. Clearly the presence of 1 wt.% Ni/AC catalyst increases the reduction of 1 wt.% $Rh/\gamma\text{-}Al_2O_3$ and MoO_3 catalysts in presence of hydrogen flow.

4. Discussion

Comparison between pure and mixed catalysts shows clearly a difference in their activity. The amount of methane produced in $\mu mol\,g^{-1}$ in the mixture formed by (25:75)Rh1Ni catalysts is 4 times higher to pure 1 wt.% $Rh/\gamma\text{-}Al_2O_3$ catalyst and 16 times to the predicted value based on the fraction of 1 wt.% $Rh/\gamma\text{-}Al_2O_3$ catalyst in the mixing. This increase cannot be due to the catalytic performances of 1 wt.% Ni/AC catalyst because no methane production was observed for it. Mixing 1 wt.% $Rh/\gamma\text{-}Al_2O_3$ and 1 wt.% Ni/AC appears to induce a significant synergy in CO_2 methanation. The synergy is lower in the other mixtures. This synergy effect could be explained by the sharing of two main properties of each catalyst: hydrogen adsorption and activation for nickel catalyst and CO_2 adsorption and dissociation for rhodium catalyst. Note that only methane and water are produced for all catalysts. Methane is then produced in all cases with a 100% of selectivity in hydrocarbon. Moreover, previously we have shown, by thermodynamic calculations, that only CH_4 and water can be produced under these experimental conditions [2]. No CO, alcohols, or other hydrocarbons could be expected to be formed. Also, reverse water gas shift reaction (RWGS) can be excluded at the reaction temperature. This endothermic reaction is promoted at higher temperature [30].

4.1. Solid state aspects of pure catalysts and mixtures of catalysts

Characterization of mixed catalysts shows no modifications at the surface (XPS) and on the first molecular layer (ToF-SIMS) when mechanical mixture is prepared, reduced or tested. The characterization results are the same when 1 wt.% $Rh/\gamma\text{-}Al_2O_3$ is alone or in the mixture with Ni/AC. These results strongly suggest that the catalysts in the mechanical mixtures can be considered as particles joint together without any chemical modification occurring during their synthesis, the reduction treatment or catalytic reaction. Thus, synergy effect can not be explained by the formation of a new phase containing Rh and Ni, or new structures formed between the metal and the surface as Rh–Al–O or Ni–Al–O or Rh–C. ToF-SIMS results are very conclusive on these aspects. In addition the XPS Rh/Al and Ni/AC atomic ratio after reduction and after test were the same when 1 wt.% $Rh/\gamma\text{-}Al_2O_3$ or 1 wt.% Ni/AC are pure or in the mixture. Then, it could be suggested that the observed synergy could be explained by a cooperative effect between both catalysts in good contact and not by chemical modifications between the catalysts.

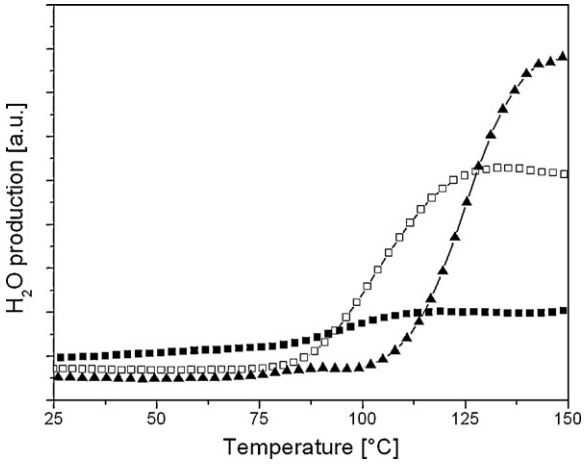

Fig. 4. H_2O–TPR profiles of 1 wt.% Rh/Al_2O_3 (□), 1 wt.% Ni/AC (■) and (50:50)Rh1Ni (▲). The catalyst mixture induces a growing up of water production. This observation suggests a better reduction of rhodium particles due to the presence of nickel particles.

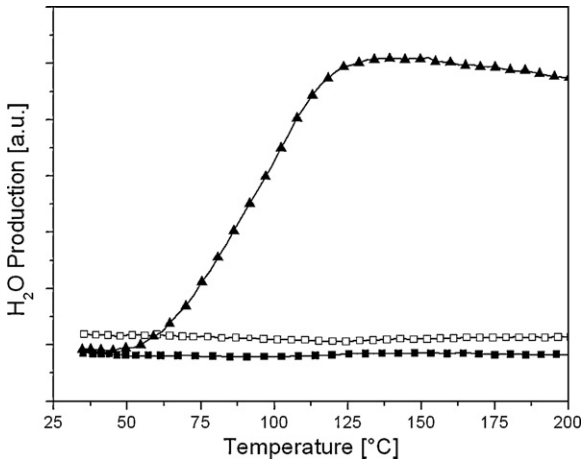

Fig. 5. H_2O–TPR profiles of MoO_3 (□), 1 wt.% Ni/AC (■) and (50:50)Mo1Ni (▲). While no water production is observed for MoO_3 and 1 wt.% Ni/AC catalysts alone, large amount of water is produced by mechanically mixed catalysts. Nickel catalyst improves hydrogen activation and reduction.

Table 8
XPS analysis of samples before and after TPR analysis of 1 wt.% Rh/γ-Al_2O_3, MoO_3 and the mixture (50:50)Mo1Ni.

Sample	Treatment	Ni/C	C/Mo	Ni/Mo	Mo^{5+}/Mo_{tot}
MoO_3	After synthesis	*	0.0023		5%
MoO_3	After reduction at 150 °C	*	0.0023		7%
1 wt.% Ni/AC	After synthesis	0.09	*		*
1 wt.% Ni/AC	After reduction at 150 °C	0.05	*		*
(50:50)Mo1Ni	After synthesis	0.04	0.0018	7.2×10^{-5}	4%
(50:50)Mo1Ni	After reduction at 150 °C	0.04	0.0017	6.8×10^{-5}	7%

* No peak.

4.2. Adsorption of CO_2

1 wt.% Rh/γ-Al_2O_3 catalyst is known for its good properties on CO_2 adsorption [4,10,11,22,31,32]. In the present study, CO_2 chemisorption experiments on 1 wt.% Rh/γ-Al_2O_3 confirm this adsorption capacity. More than half of the CO_2 adsorbed in the catalysts is adsorbed on alumina support. Rhodium deposition increases CO_2 adsorption. The behavior of nickel catalyst is very opposite: no CO_2 adsorption occurs on pure activated carbon and on the 1 wt.% Ni/AC catalyst. The absence of catalytic activity of 1 wt.% Ni/AC can be easily relying to this absence of adsorption of CO_2. Nevertheless, literature shows that CO_2 adsorption and dissociation can occur on nickel deposit in Al_2O_3 and SiO_2 [12,18–20,24]. As for 1 wt.% Rh/γ-Al_2O_3, the support plays the crucial role in CO_2 adsorption on nickel catalysts.

As already mentioned, the adsorption of CO_2 is a crucial step for its methanation. Indeed, it is known that CO_2 adsorption is the first step of the catalytic cycle [2,11,21,22]. The second step is the CO_2 dissociation in CO and O on the surface [3,10,11,13,14,21,22,31,32]. CO_2 dissociation is the rate-limiting step. In fact, CO_2 dissociation is influenced by CO coverage on the surface and the strength of the bond Rh—CO [11,21]. All these steps in CO_2 methanation are assisted by hydrogen and mainly, the CO_2 dissociation [4]. It has been claimed that the CO formation from CO_2 seems facilitated by the formation of formate species adsorbed on the surface [6]. On the other hand, H_2 can react with CO to produce methane or water [2,3,11,14], displacing the equilibrium allowing to adsorb and dissociate more CO_2. But, the hydrogen adsorption at the surface is in competition with CO_2 adsorption. Due to the preferential adsorption of CO_2 and the accumulation of CO on the surface, hydrogen coverage on rhodium catalyst is very small. Inversely, H_2 is easily adsorbed on 1 wt.% Ni/AC catalyst [26] and CO_2 is not adsorbed at all.

4.3. Catalytic cooperation between catalysts

Catalytic cooperation could be explained by the transfer of activated reactant species from one phase to another. The transfer of some intermediates seems difficult to be accepted. Indeed, DRIFT experiments on 1 wt.% Rh/γ-Al_2O_3 catalysts showed that CO_2 is adsorbed dissociatively, forming gem-dicarbonyl $Rh(CO)_2$ and Rh–CO linear species. These species are hydrogenated to form methane. No other species on the surface was formed. In addition, the type of adsorbed species depends on the rhodium oxidation state [2]. As a first explanation, it could be assumed that these dissociated species are transferred from 1 wt.% Rh/γ-Al_2O_3 catalyst to 1 wt.% Ni/AC catalyst. Meanwhile it is important to emphasize that no CO_2 adsorption and CH_4 production occur on 1 wt.% Ni/AC. Then the hypothesis of a transfer of dissociated species from 1 wt.% Rh/γ-Al_2O_3 to 1 wt.% Ni/AC catalysts can be reasonably excluded. Another alternative to explain the synergy observed is the hydrogen migration from 1 wt.% Ni/AC toward 1 wt.% Rh/γ-Al_2O_3. Hydrogen migration by spill-over mechanism has already been proved on Ni/AC catalyst in the hydrogenation of benzene [26]. Hydrogen adsorption and storage was hardly proved in nickel catalysts supported on activated carbon and the best results are obtained with 1 wt.% Ni/AC[25]. Ni/AC could store significant amounts of hydrogen at room temperature and high pressure. The hydrogen molecules dissociated on the metal phase, migrate by spill-over mechanism from the metal onto the support where they are strongly adsorbed. Moreover, they can be desorbed through the reverse spill-over effect that is the migration of H atoms from the support onto the metal phase where they recombine and desorb. Moreover, Park et al. suggested a hydrogen spill-over on Pd–Mg/SiO_2 catalyst applied on CO_2 methanation [24]. Also, Teichner et al. demonstrated that alumina is a good acceptor of hydrogen spill-over [33]. In rhodium–nickel catalysts mixing, hydrogen species could move from 1 wt.% Ni/AC to 1 wt.% Rh/γ-Al_2O_3 catalysts particles and improve the methanation rate. Clearly it seems that an external feeding of hydrogen might improve catalytic performances by bypassing the hydrogen adsorption competition at the surface of Rh/γ-Al_2O_3 catalyst.

Experimental evidences of a migration of hydrogen between phases in the mixture could come from TPR and XPS analysis. Fig. 5 exhibits clearly the promoter effect of mixing 1 wt.% Ni/AC with MoO_3 in TPR analysis. The XPS Ni/Mo atomic ratio and the Ni binding energy, before and after TPR, remain unchanged, excluding any surface contamination between the MoO_3 and Ni/AC particles. The formation of Ni–Mo–O structures or a contamination of the pure solid during the TPR treatment seems to be excluded. The water production in the mixture increases significantly compared with alone MoO_3. Clearly Ni/AC catalyst improves the reduction of MoO_3. This result is explained by the transfer of hydrogen from 1 wt.% Ni/AC toward MoO_3. The consequence is a reduction of the oxide and thus, an increase in water production. It is necessary to underline that similar results were observed during TPR of 1 wt.% Rh/γ-Al_2O_3 catalyst and the mixture (50:50)Rh1Ni.

After catalytic test, the XPS analyses of the 1 wt.% Rh/γ-Al_2O_3 catalyst and the mixture (50:50)Rh1Ni show that the percentage of rhodium oxidized is the same when 1 wt.% Rh/γ-Al_2O_3 works alone or in the mixture. In both cases rhodium atoms are reduced during reduction step and oxidized to a similar value during the reaction. Even on strong reductive conditions, a slight re-oxidation of rhodium particles is possible by the presence of CO_2 and its dissociation. Moreover, the oxidation potential of CO_2 has already been proved by Demoulin et al. [34]. Nevertheless rhodium particles remain always in a reduced state (about 65%). The hydrogen transferred from the Ni/AC to 1 wt.% Rh/γ-Al_2O_3 could have two effects. Firstly is to keep Rh particles in a reduced state and secondly is to participate directly in the reaction. The first alternative seems to be supported by TPR results with MoO_3. However it is necessary to recognize that MoO_3 is an oxide highly reducible, more reducible than Rh oxide. As concern the second alternative, namely the direct participation in the reaction of the hydrogen transferred, previous study suggests that C—O bond breaking by hydrogen is a key step in the reaction and probably the rate determining step of the reaction [4]. Study of the influence of size particles proposes that the lateral faces of the Rh

particles could play a crucial role in the reaction mechanism. The formation of hydrogen species promotes the formation of Rh carbonyl hydride. In fact, H atom of Rh carbonyl hydride enhances the strength of Rh—C bond while decreasing the strength of C—O bond. This increases the rate of CO dissociation and then the methanation rate [4]. These results could indicate that in the present case, hydrogen species supplied by the Ni/AC catalysts could play exactly the same role than hydrogen activated in lateral phases of Rh particles. These hydrogen species irrigate the surface of Rh particles and promote the formation of carbonyl hydride.

Note that TPR results at 125 °C presented in Fig. 4 show no difference in the reduction rate of 1 wt.% Rh/γ-Al_2O_3 alone or in mixtures. The synergetic effect would be not due to an increase in the reduction rate of Rh particles. More probably the main effect is the surface transfer of hydrogen to facilitate the hydrogenation of the CO adsorbed species in CH_4.

4.4. Influence of nickel content

Results obtained using mixtures of 1 wt.% Rh/γ-Al_2O_3 with Ni/AC catalyst containing 0.5% and 5% of Ni confirm the important role of the Ni content in catalysts in the methanation reaction. From Table 1 it is clearly observed that the Ni content in the catalyst influences the formation of methane. On one hand, 0.5 wt.% of nickel appears not enough to induce an enhancement of activity. In another hand, 2.5 wt.% of nickel (according to ICP-AES results for 5 wt.% Ni/AC sample) is active in methanation. In that case, we could suppose that activated hydrogen is directly used on nickel catalyst to produce methane without transfer to rhodium particles. Otherwise, even if the size of nickel particles is unknown, according to Wojcieszak et al. [26], the size of 1 wt.% Ni/AC would be very small. Authors observed that high dispersion and high catalytic performances are favored by a low nickel content (study on 1 wt.%, 5 wt.% and 10 wt.% nickel content). This small size combined with the higher surface area (Table 3) is suggested to enhance the storage of hydrogen in the nickel catalyst [25]. According to chemisorption results and literature data, an important adsorption of CO_2 on 1 wt.% Rh/γ-Al_2O_3 occurs. We suspect with (75:25) and (50:50) mixture that the hydrogen supply from 1 wt.% Ni/AC is not enough to change drastically the CO_2 conversion to methane. In the case of (25:75)Rh1Ni catalyst, the high adsorption ability of CO_2 on Rh catalyst joint with the higher hydrogen feeding induces the most marked synergy effect.

4.5. Hydrogen supply

An important result is obtained when the carrier H_2 was changed by He. The catalyst is first reduced by pre-treatment under hydrogen and followed by a pulse of CO_2 carried out by a He flow instead of H_2. In this case no production of methane is observed. The presence of H_2 in the gaseous atmosphere is then crucial for the methanation. Indeed, it could be claimed that during the reduction step, the Rh is reduced and a part of hydrogen is still adsorbed on the surface after the process. Then it could be expected that reduced Rh has enough hydrogen species to hydrogenate, at least during a short time, the CO_2 dissociated on the surface of the catalyst. This was not the case. Then, we can suggest that the hydrogen necessary for the reaction is not the same hydrogen than H_2 adsorbed during the reduction step. During the reaction, a different specie of hydrogen is formed which allows the hydrogenation of the adsorbed CO to methane. In the CO_2 methanation mechanism, it seems to be needful to adsorb and activate firstly CO_2. Hydrogen reacts in a second time. It can come from hydrogen activated on different faces of Rh particles or from hydrogen, as in our present case, supplied by an external phase, as Ni/AC.

5. Conclusions

Mechanical mixtures of Rh/γ-Al_2O_3 and Ni/AC catalysts prepared separately, show a significant catalytic synergy in the methanation of CO_2. This effect is more important when the content of Ni is 1 wt.%. The production of methane is higher compared with the methane formation observed with the pure catalysts. Physicochemical characterizations of the catalysts are the same when they are alone or mixed together mechanically. There is no chemical contamination or formation of new structures when the catalysts are mixed. The synergy is explained by cooperation between the two catalysts during methanation. Particularly, 1 wt.% Rh/γ-Al_2O_3 is highly efficient in CO_2 adsorption. On the other hand, 1 wt.% Ni/AC catalyst is able to absorb a high quantity of hydrogen and very little carbon dioxide. These properties joint together by a simple mixing catalyst induce an increase of carbon dioxide conversion and methane formation. In all cases only methane is formed. The augmentation of the catalytic performances would be attributed to a migration of activated hydrogen species from 1 wt.% Ni/AC catalysts toward 1 wt.% Rh/γ-Al_2O_3. This hydrogen can then react with CO_2 species to form methane but also to preserve rhodium particles in an adequate reduced state essential for CO_2 hydrogenation. This concept could be applied to other reactions which need a modulate supply of hydrogen, in particular in catalysis where adsorption competition exists between hydrogen and another reactant.

Acknowledgments

The authors thank M.J. Genet for his fruitful advices about XPS technique. The authors gratefully acknowledge the "Direction Générale des Technologies, de la Recherche et de l'Energie (DGTRE)" of the "Région Wallonne" (Belgium), the "Fonds National de la Recherche Scientifique (FNRS)" of Belgium, for their financial support. The involvement of "Unité de catalyse et de chimie des matériaux divisés" (IMCN, MOST) in the "INANOMAT" IUAP network sustained by the "Service public fédéral de programmation politique scientifique" (Belgium) is acknowledged. M.J. and C.S. are grateful to the FRIA (Belgium) for their PhD student positions.

References

[1] H. Yang, Z. Xu, M. Fan, R. Gupta, R.B. Slimane, A.E. Bland, I. Wright, Journal of Environmental Sciences 20 (2008) 14–27.
[2] A. Beuls, C. Swalus, M. Jacquemin, G. Heyen, A. Karelovic, P. Ruiz, Applied Catalysis B: Environmental 113–114 (2012) 2–10.
[3] M. Jacquemin, A. Beuls, P. Ruiz, Catalysis Today 157 (2010) 462–466.
[4] A. Karelovic, P. Ruiz, Applied Catalysis B: Environmental 113–114 (2012) 237–249.
[5] A. Lattes, De l'hydrogénation catalytique à la théorie chimique de la catalyse: Paul Sabatier, chimiste de génie apôtre de la décentralisation, Elsevier, Paris, France, 2000.
[6] W. Wei, G. Jinlong, Frontiers of Chemical Science and Engineering 5 (2011) 2–10.
[7] G. Centi, S. Perathoner, Studies in Surface Science and Catalysis 153 (2004) 1–8.
[8] S.-E. Park, J.-S. Chang, K.-W. Lee, Studies in Surface Science and Catalysis 153 (2004) 626.
[9] D.J. Dwyer, G.A. Somorjai, Journal of Catalysis 52 (1978) 291–301.
[10] B.A. Sexton, G.A. Somorjai, Journal of Catalysis 46 (1977) 167–189.
[11] F. Solymosi, A. Erdöhelyi, T. Bánsági, Journal of Catalysis 68 (1981) 371–382.
[12] G.D. Weatherbee, C.H. Bartholomew, Journal of Catalysis 77 (1982) 460–472.
[13] F. Solymosi, I. Tombácz, J. Koszta, Journal of Catalysis 95 (1985) 578–586.
[14] Z.L. Zhang, A. Kladi, X.E. Verykios, Journal of Catalysis 148 (1994) 737–747.
[15] X.E. Verykios, Applied Catalysis A 255 (2003) 101–111.
[16] F. Solymosi, A. Erdohelyi, M. Kocsis, Journal of the Chemical Society, Faraday Transactions 1 (77) (1981).
[17] M.R. Prairie, A. Renken, J.G. Highfield, K. Ravindranathan Thampi, M. Grätzel, Journal of Catalysis 129 (1991) 130–144.
[18] T. Van Herwijnen, H. Van Doesburg, W.A. De Jong, Journal of Catalysis 28 (1973) 391–402.
[19] J.L. Falconer, A.E. Zağli, Journal of Catalysis 62 (1980) 280–285.
[20] S.-i. Fujita, M. Nakamura, T. Doi, N. Takezawa, Applied Catalysis A 104 (1993) 87–100.

[21] M.R. Prairie, J.G. Highfield, A. Renken, Chemical Engineering Science 46 (1991) 113–121.
[22] M.F.H. van Tol, A. Gielbert, B.E. Nieuwenhuys, Applied Surface Science 67 (1993) 166–178.
[23] F. Solymosi, Journal of Molecular Catalysis 65 (1991) 337–358.
[24] J.-N. Park, E.W. McFarland, Journal of Catalysis 266 (2009) 92–97.
[25] M. Zieliński, R. Wojcieszak, S. Monteverdi, M. Mercy, M.M. Bettahar, International Journal of Hydrogen Energy 32 (2007) 1024–1032.
[26] R. Wojcieszak, M. Zieliński, S. Monteverdi, M.M. Bettahar, Journal of Colloid and Interface Science 299 (2006) 238–248.
[27] J.H. Scofield, Journal of Electron Spectroscopy and Related Phenomena 8 (1976) 129–137.
[28] C. Wagner, W. Riggs, L. Davis, J. Moulder, G. Muilenberg, Handbook of X-ray Photoelectron Spectroscopy, Perkin-Elmer Corporation, Physical Electronics Division, 1979.
[29] P. Bertrand, L.-T. Weng, Mikrochimica Acta 13 (1996) 167–182.
[30] E.D. Park, D. Lee, H.C. Lee, Catalysis Today 139 (2009) 280–290.
[31] D.G. Castner, B.A. Sexton, G.A. Somorjai, Surface Science 71 (1978) 519–540.
[32] F. Solymosi, P. Tolmacsov, K. Kedves, Journal of Catalysis 216 (2003) 377–385.
[33] M. Lacroix, G.M. Pajonk, S.J. Teichner, Journal of Catalysis 101 (1986) 314–322.
[34] O. Demoulin, M. Navez, J.L. Mugabo, P. Ruiz, Applied Catalysis B: Environmental 70 (2007) 284–293.